

RESEARCH

Open Access



H3K18 lactylation-mediated nucleotide-binding oligomerization domain-2 (NOD2) expression promotes bilirubin-induced pyroptosis of astrocytes

Jing Li^{1,2}, Siyu Li^{1,2}, Qian Sun^{1,2}, Ling Li^{1,2}, Yan Zhang² and Ziyu Hua^{1,2*}

Abstract

Histone lactylation, a newly glycosis-related histone modification, plays a crucial role in the regulation of gene expression in various immune cells. However, the role of histone lactylation in astrocytes remains unclear. Here, this study showed that the H3K18 lactylation (H3K18la) levels were upregulated in primary astrocytes under unconjugated bilirubin (UCB) stimulation and hippocampus of bilirubin encephalopathy (BE) rats. Inhibition of glycolysis decreased H3K18la and attenuated pyroptosis both in vitro and in vivo. CUT& Tag and RNA-seq results revealed that H3K18la was enriched at the promoter of nucleotide-binding oligomerization domain 2 (NOD2) and promoted its transcription. Moreover, NOD2 boosted the activation of downstream mitogen-activated protein kinase (MAPK) and nuclear factor-kappa B (NF- κ B) signaling pathways, which exacerbated the neuroinflammation of BE. Collectively, this study provides a novel understanding of epigenetic regulation in astrocytes, and interruption of the H3K18la/NOD2 axis may represent a novel therapeutic strategy for treating bilirubin encephalopathy.

Introduction

Neonatal hyperbilirubinemia is a common clinical phenomenon that results from both physiological and pathological causes (1, 2), which is estimated to occur in 60% of term and 80% of preterm neonates (3, 4). Bilirubin encephalopathy (BE) is defined as the presence of acute or chronic neurologic dysfunction associated with severe hyperbilirubinemia. Chronic bilirubin encephalopathy, also known as kernicterus, is characterized by neurodeafness, cerebral palsy and mental retardation [5]. The epidemiology of BE varies greatly across regions and populations studied. Despite the significant reduction of

BE incidence worldwide, rate of kernicterus still remains particularly high in low- and middle-income countries (LMIC) due to lack of timely and rapid interventions (6, 7). Recently, increasing evidence indicates that inflammation plays a critical role in the neurotoxicity induced by unconjugated bilirubin (UCB) [8–10]. Specifically, high levels of UCB triggered glial cell reactivity, causing the release of pro-inflammatory factors (such as interleukin (IL)-1 β , tumor necrosis factor alpha (TNF- α), and IL-6) in the same way as lipopolysaccharide (LPS) (11, 12). Pyroptosis, a highly inflammatory form of programmed cell death, is characterized by membrane pore formation, osmotic swelling, DNA damage, and the massive release of cytoplasmic contents and inflammatory mediators [13]. Our previous in vivo and in vitro research confirmed that pyroptosis was involved in the process of UCB-induced neurotoxicity (14, 15). However, the upstream

*Correspondence:

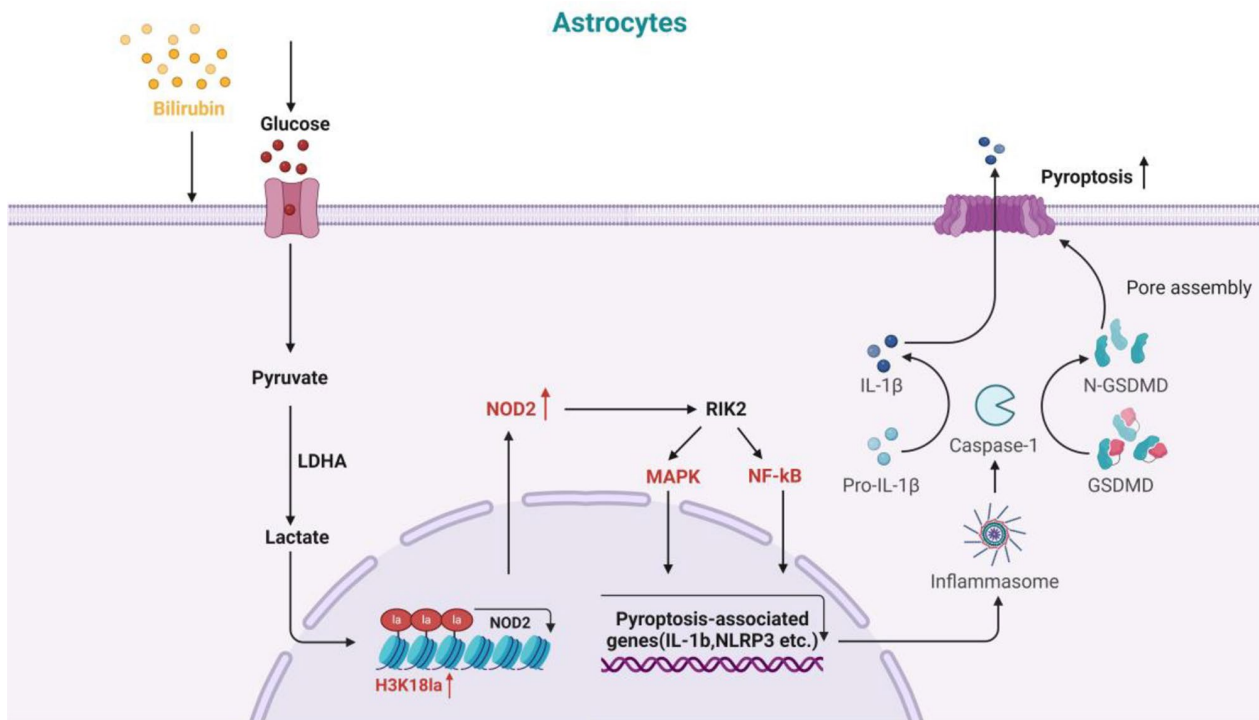
Ziyu Hua
h_ziyu0517@163.com

Full list of author information is available at the end of the article



© The Author(s) 2025. **Open Access** This article is licensed under a Creative Commons Attribution-NonCommercial-NoDerivatives 4.0 International License, which permits any non-commercial use, sharing, distribution and reproduction in any medium or format, as long as you give appropriate credit to the original author(s) and the source, provide a link to the Creative Commons licence, and indicate if you modified the licensed material. You do not have permission under this licence to share adapted material derived from this article or parts of it. The images or other third party material in this article are included in the article's Creative Commons licence, unless indicated otherwise in a credit line to the material. If material is not included in the article's Creative Commons licence and your intended use is not permitted by statutory regulation or exceeds the permitted use, you will need to obtain permission directly from the copyright holder. To view a copy of this licence, visit <http://creativecommons.org/licenses/by-nc-nd/4.0/>.

Graphical abstract



Keywords Astrocytes, Glycolysis, H3K18 lactylation, Bilirubin, Neuroinflammation

regulators of pyroptosis in BE are not well-understood, so the potential regulatory mechanisms need to be further investigated to develop new therapeutic strategies.

As the most abundant glial cells in the brain, astrocytes play a significant role in neuroinflammatory process [16–18]. With the development of the new field of “immunometabolism”, some existing evidence has already verified the interconnections in astrocytes between metabolism adaptations and inflammatory responses. Among *in vivo* and *in vitro* studies, increased glycolysis and lactate release in astrocytes were discovered in response to inflammatory insults, and inhibition of glycolysis reduced cytokine release and nuclear factor-kappa B (NF-κB) activity [19–23], which indicate that intact glycolysis is necessary for the full inflammatory of astrocytes response to various stimuli. Additionally, lactate, the product of aerobic glycolysis, can directly stimulate astrocytes to release pro-inflammatory factors, although the response was not as strong as that of microglia [24]. According to our preliminary research, the pyroptosis of astrocytes was implicated in UCB-induced neuroinflammatory injury [14, 15], but the metabolic changes of astrocytes during this process and its impact on pyroptosis remain unclear. Interestingly, a recent study found that lactate levels in various brain areas of newborn rats

subjected to bilirubin were significantly elevated relative to the controls [25]. As the energy regulatory center of the brain, astrocytes are typical cells responsible for processing glucose through aerobic glycolysis [26], and most likely account for the relatively high glycolytic capacity of brain tissue [27, 28]. Therefore, it is reasonable to assume that astrocytes exposed to UCB undergo metabolic changes which probably contribute to cell pyroptosis, and the underlying mechanisms are unknown.

Chromatin posttranslational modifications (PTMs), or epigenetic changes, play essential roles in regulating cellular plasticity in a heritable, reversible, and fine manner [29]. Recent findings have identified a variety of cellular metabolites can act as substrates for PTMs, leading to diverse types of lysine acetylation modifications, such as crotonylation, malonylation, succinylation, and β-hydroxybutyrylation etc [30]. Lactate, originally considered a byproduct of anaerobic metabolism, is increasingly being explored as a signaling molecule and substrate of PTMs to carry out biological functions. In 2019, Zhang et al. [31] for the first time discovered a new type of histone acylation modification using lactate as a substrate, called histone lactylation, that can regulate gene expression directly. Subsequently, a growing number of studies have found that histone lactylation affects

gene transcription in various physiological and pathological processes, including stem cell differentiation, embryonic development, inflammation and immune response, neoplastic disease and neuropsychiatric disorders, among which H3K18 lactylation (H3K18la) is the most widely studied [32].

Many studies have reported that H3K18la plays pro-inflammatory roles in inflammation and immune response. Chu et al. [33] observed that H3K18la levels of peripheral blood mononuclear cells in septic shock patients were higher than that in non-septic shock patients and healthy controls, and H3K18la expression levels were positively correlated with sepsis severity and prognosis. In Alzheimer's disease (AD), enhanced H3K18la was observed in senescent microglia, which dramatically impacted brain aging and AD pathology through potentiating NF- κ B signaling [34]. In another study, H3K18la was demonstrated to induce pyroptosis in the oxygen-glucose deprivation/reoxygenation (OGD/R) treated N2a cells [35]. Collectively, these studies indicate that H3K18la plays pivotal roles in modulating the process of neuroinflammation. However, little is known about the potential roles of H3K18la in inflammatory activation of astrocytes (e.g., pyroptosis) as well as the possible mechanisms involved. Thus, the present study aimed to determine whether H3K18la is involved in astrocyte pyroptosis and its detailed downstream regulatory mechanisms.

Materials and methods

Animals

Eight-week-old adult Sprague–Dawley (SD) rats (weighing 250–280 g) were purchased from the Experimental Animal Center of Chongqing Medical University. All rats were maintained in a light- and temperature-controlled specific pathogen-free (SPF) animal facility (23 ± 2 °C, a 12 h light/dark cycle) with free access to food and water. For breeding, one male rat cohabited with three females at a ratio of 1:3, and the neonatal rats born from the pregnancies were used in subsequent experiments. A total of about 220 neonatal rats were used in this study, of which 72 were used for cellular experiments, 30 for immunohistochemistry (IHC) experiments, 26 for behavioral tests and 92 for other *in vivo* experiments. The animal studies were conducted in compliance with the Guide for the Care and Use of Laboratory Animals of the National Institutes of Health.

Primary astrocytes culture and treatment

Astrocytes were harvested from the cerebral cortex of 1 to 3 days neonatal rats as described previously [36]. Briefly, following removal of the meninges and blood vessels, the isolated cerebral cortex was digested with 0.125% trypsin (Sigma-Aldrich, USA) and 0.1 mg/mL

Deoxyribonuclease I (Sigma-Aldrich, USA) at 37 °C for 30 min, and terminated with Dulbecco's modified Eagle medium (DMEM, Gibco, USA) containing 10% fetal bovine serum (FBS, ExCell, China) and 1% penicillin–streptomycin. After centrifugation and resuspension, the cell suspensions were filtered through a nylon mesh (diameter, 70 μ m) and cultured in T75 cell culture flasks (1 brain per flask). The cells were maintained in a humidified incubator at 37 °C containing 5% CO₂. The medium changes were performed every three days with DMEM complete medium.

The primary astrocytes were used when more than 95% of the cells were stained positively for the astrocytic marker glial fibrillary acidic protein (GFAP). The bilirubin powder (Sigma-Aldrich, USA) was pre-dissolved in dimethylsulfoxide (DMSO, Sigma-Aldrich, USA) solution (10 mM/L). The astrocytes in the UCB group were treated with 50 μ mol/L bilirubin solution in the presence of 100 μ mol/L human serum albumin (HSA, Sigma-Aldrich, USA), which mimicked the neonatal hyperbilirubinemia conditions [37, 38]. To avoid photodegradation, all experiments with UCB were conducted away from light. In addition, the control group received equal volumes of DMSO and HSA.

BE model establishment and treatment

As described previously, the rat BE model was established by the same method [39]. Briefly, the SD rat pups were anesthetized with 1.5–2.0% isoflurane inhalation on postnatal day 3, and then a small amount of cerebrospinal fluid (CSF) was released from the cisterna magna (CM) to prevent intracranial hypertension using a microsyringe. After that, the same amount of bilirubin (10 μ g/g body weight) or control solution was injected into the CM. Bilirubin powder was solubilized in a 0.05 M NaOH solution, and the pH of the NaOH solution prepared for control solution was adjusted to 8.5 with HCl (0.05 M). To inhibit lactate production, sodium oxamate (OX, 0.5 g/kg body weight) was administered intraperitoneally 6 h before UCB injection. For blocking the NOD2 production, neonatal rats were intraperitoneally injected with GSK717 (10 g/kg body weight) one day prior to the UCB challenge.

Seahorse analysis

Cellular metabolic changes were determined using a Seahorse XFe96 Extracellular Flux Analyzer and a Seahorse XF Glycolytic Rate Assay Kit (Agilent, USA) following the manufacturer's instructions. All compounds and materials were sourced from Agilent Technologies. Briefly, primary cultured astrocytes were seeded at a concentration of 2×10^4 cells/well on 96-well Seahorse XF cell culture microplates in DMEM complete medium for 3 days. Prior to the assay, the cells were washed and incubated

in Seahorse XF DMEM medium containing 10 mM glucose, 1 mM pyruvate and 2 mM glutamine for 45 min at 37 °C without CO₂. To evaluate basal and compensatory glycolysis, the proton efflux rate (PER) response following injections of the electron transport chain inhibitors rotenone/antimycin A (ROT/AA) and the glucose analog 2-DG was measured. The extracellular acidification rate (ECAR), PER and glycolytic proton excretion rate (Glyco-PER) were then calculated using the Seahorse Glycolytic Rate Assay Report Generator.

Measurement of lactate levels

After re-suspended with pre-cooled PBS, digested astrocytes and isolated hippocampal tissue were sonicated on ice at 300 W (on for 5~7 s, off for 10s) for 4~5 times, and then centrifuged at 13,000 rpm for 10 min at 4 °C. The supernatants were collected, and the lactate levels were measured using a Lactic Acid assay kit (Nanjing Jiancheng Bioengineering Institute, China) based on the manufacturer's instructions.

Western blot

Total protein was extracted from brain tissues and cultured primary astrocytes with RIPA buffer (Beyotime Biotechnology, China) containing phosphatase and protease inhibitors (Beyotime Biotechnology, China). The supernatants were collected following sonication and centrifugation, and protein concentrations were detected with the BCA protein assay kit (Beyotime Biotechnology, China). The samples were separated by sodium dodecyl sulfate-polyacrylamide gel electrophoresis (SDS-PAGE), and transferred onto polyvinylidene difluoride (PVDF) membranes (Millipore, USA). After blocked with 5% skim milk for 1 h at room temperature, the PVDF membranes were incubated with primary antibodies overnight at 4 °C on a shaker. The following antibodies were used in this experiment: H3K18la (1:2000, PTM1406RM, PTM BIO, China), the NOD-like receptor family pyrin domain containing 3 (NLRP3) (1:500, NBP2-12446, Novus, USA), Caspase-1 p20 (1:2000, 22915-1-AP, proteintech, China), gasdermin D N-terminal (GSDMD-N) (1:1000, ab219800, Abcam, USA), Histone 3 (1:2000, 9715 S, CST, USA), β -actin (1:5000, A5441, Sigma-Aldrich, USA), receptor-interacting protein kinase 2 (RIK2) (1:2000, 15366-1-AP, proteintech, China), p-p65 (1:2000, 82335-1-RR, proteintech, China), c-Jun-N-terminal-kinase (JNK) (1:1000, R24780, zenbio, China), p-JNK (1:1000, R381100, zenbio, China), p-38 (1:2000, 14064-1-AP, proteintech, China), p-p38 (1:2000, 28796-1-AP, proteintech, China), extracellular signal-regulated kinase 1/2 (ERK) (1:2000, 11257-1-AP, proteintech, China) and p-ERK (1:2000, 28733-1-AP, proteintech, China), α -tubulin (1:5000, ER130905, HUA-BIO, China), NOD2 (1:2000, 54121, SAB, USA). Afterwards, the membranes were incubated with the

appropriate horseradish peroxidase-labelled secondary antibodies (1:5000, ZB-2305/ZB-2301, ZSGB-Bio, China) at room temperature for 1 h. Finally, the protein bands were visualized with the Bio-Rad ChemiDoc MP Imaging System and quantified with ImageJ software.

Cell counting kit-8 (CCK8) assay

Cell viability was assessed using Cell Counting Kit-8 (APExBIO, USA) according to the manufacturer's instructions. Primary astrocytes were plated in 96-well plates at 3×10^4 cells/well density, and CCK-8 solution was added into each well after indicated treatment, followed by incubation for indicated periods of time at 37 °C. Cell survival rate was finally determined by measuring the absorbance at 450 nm with a microplate reader.

Immunofluorescence (IF) and H&E staining

The brains of rats were isolated after transcardial perfusion, and then fixed with 4% paraformaldehyde (PFA) at 4 °C overnight. Dehydration was performed with 30% sucrose at 4 °C for about 2 days. After embedded in an optimal cutting temperature compound (Sakura Finetek, Japan), the brain tissues were sliced into 30- μ m sections for IF.

The brain slices and the cell-climbing sheets were washed with PBS prior to fixation with PFA at room temperature. Subsequently, the brain sections were repaired with trisodium citrate and the cover slides were permeabilized with 0.1% Triton X 100, followed by BSA to seal them. The samples were incubated with primary antibody against GFAP (1: 200, 13-0300, ThermoFisher, USA), H3K18la (1:200, PTM1406RM, PTM BIO, China) and NOD2 (1: 500, 54121, SAB, USA) at 4 °C overnight, and then incubated with corresponding fluorochrome-labeled secondary antibodies for 1 h in the dark at room temperature. After stained with DAPI, the samples were mounted with an anti-fluorescence quenched sealer. Images were captured using A1R Confocal Laser Scanning Microscope (Nikon, Japan).

For H&E staining, the brain tissues were sectioned into 4 μ m-slices after dehydration and paraffin embedding. Next, H&E staining was carried out in accordance with routine procedures. Light microscopy (Nikon) was used to visualize the histopathological changes of the hippocampus and cortex.

Enzyme-linked immunosorbent assay (ELISA)

The levels of IL-1 β were tested in culture supernatants of primary astrocytes and hippocampus tissues of BE rats by ELISA kits (4 A Biotec, China) as instructed by the manufacturers. A BioTek microplate reader was used to measure samples' absorbance at a wave length of 450 nm.

Real-time quantitative polymerase chain reaction (RT-qPCR)

Total RNA was extracted from primary astrocytes and the hippocampus tissues using the SteadyPure RNA Extraction Kit (Accurate Biology, China), and reverse-transcribed to complementary DNA with the PrimeScript RT reagent Kit (Takara, Japan). Then, qPCR was carried out utilizing QuantiNova SYBR Green PCR reagents (Qiagen, Germany) as per the manufacturer's guidelines on the Bio-Rad CFX96 Real-Time PCR Detection System. β -Actin was used as the internal control for normalizing the expression of target genes, and the $2^{-\Delta\Delta Ct}$ relative quantification method was used for data analysis. The primer sequences used are shown in Additional file 1: Table S1.

RNA extraction, library construction, and illumina sequencing

Total RNA was extracted from cultured primary astrocytes using TRIzol reagent (Invitrogen, USA). The purity and concentration of RNA were evaluated by a NanoDrop 2000 spectrophotometer (Thermo Scientific, USA), and the integrity of the RNA was confirmed by the 2100 Bioanalyzer (Agilent Technologies, USA). Next, the libraries were prepared using VAHTS Universal V6 RNA-seq Library Prep Kit, and sequenced using Illumina Novaseq 6000 platform (OE Biotech Co., Ltd., Shanghai, China). The mRNA levels were normalized by the fragments per kilobase of exon model per million mapped reads (FPKM).

CUT&Tag assays and CUT&Tag qPCR

The CUT&Tag assay was conducted using the Hyperactive™ In-Situ ChIP Library Prep Kit for Illumina (Vazyme Biotech, China) in accordance with the manufacturer's instructions. After being washed with PBS, cultured primary astrocytes were incubated with ConA Beads, primary antibody against H3K181a, secondary antibody and the Hyperactive pA-Tn5 Transposase in order and then fragmented. The fragmented DNA was then isolated, amplified, and purified for sequencing and qPCR assays. For CUT&Tag sequencing, the libraries were sequenced on an Illumina NovaSeq6000 platform (OE Biotech Co., Ltd., Shanghai, China). The clean reads were obtained after removing adapter sequences and low-quality reads with Fastp software, and mapped to the rat reference genome using Bowtie2. Peak calling was performed with SEACR software and annotated using CHIPseeker software. IGV software was used to visualize peak distributions along genomic regions of interested genes. The DNA purified from CUT&Tag assay was quantified by qPCR to identify the expression levels of H3K181a-bound genes. The primer sequences employed are displayed in Additional file 1: Table S2.

Si-RNAs and plasmids transfection

Small interfering RNAs (si-RNAs) were purchased from D-Nano Therapeutics (Beijing, China). PcDNA3.1-NOD2 overexpression plasmid and pcDNA3.1-NC vector were constructed by GENE CREATE Bioengineering Co., Ltd (Wuhan, China). Plasmids were extracted by TIANprep Rapid Mini Plasmid Kit (TIANGEN, China). Si-RNAs (50 nM/L/well) and plasmids DNA (control or NOD2 plasmid, 3 μ g/well) were transfected into cultured primary astrocytes in 6-well plates using CALNP RNAi in vitro transfection reagent (D-Nano Therapeutics, China) and Polyethylenimine linear (PEI) (APEX BIO, USA), respectively. For transfection involving both si-RNAs and plasmids, the cells were transfected with plasmids for 6 h before transfection with si-RNAs. After 48 h, the cells were collected for further experiments. To exclude cellular genetic alterations induced by transfection reagent or stimulation by si-RNA sequences, si-NC (50 nM/L/well) was transfected as a negative control which consisted of a segment of nonsense sequence. The sequences of si-RNAs are listed in Additional file 1: Table S3.

Morris water maze

The Morris water maze test was assessed at the age of 28 days. Before experiments, the rats were acclimated for 30 min in the experimental environment. The Morris water maze test was used to evaluate the rats' spatial learning and memory abilities. A black circular pool (150 cm diameter, 550 cm high) was divided in four imaginary quadrants with four equidistant graphics on the pool's inner wall, and the water temperature was maintained at 25 ± 1 °C. A platform was put inside the target quadrant of this pool 1.0 cm below the water surface. During the five subsequent days, the rats were given four trials each day with at least 30 min interval between training sessions. For each training trial, rats were put into the pool in different quadrants for a maximum time of 60 s. Rats were permitted to stay on the platform for 10 s once they found it in 60 s. Otherwise, they were guided onto the platform and stayed there for 10 s. On the sixth day, the platform was removed from the pool and rats were given a 60-sec free swim. In each trial, time spent in the targeted quadrant and number of platform crossings were recorded by the ANY-maze software.

Statistical analysis

Data analysis and graph construction were performed using *GraphPad Prism* 9.0. Data were obtained from at least three independent biological replicate experiments. The continuous variables were presented as mean \pm standard deviation (SD) after being tested for normality. Student's t-tests were used to analyze statistical differences between two experimental groups, and one-way analysis of variance (ANOVA) followed by *Tukey's* multiple

comparisons test was used for multiple groups. The categorical data were analyzed by χ^2 test. $P < 0.05$ was considered statistically significant.

Results

UCB increased lactate and H3K181a levels in primary cultured astrocytes, and hippocampus of BE rats

GFAP staining revealed that the purity of primary cultured astrocytes was more than 95%, allowing them to be used for the following experiments (Fig. 1A). To assess the metabolic switch, the time-dependent changes of lactate and H3K181a levels in primary cultured astrocytes exposed to UCB and hippocampus of BE rats were initially examined. The colorimetric assay indicated that the lactate levels in UCB-treated primary cultured astrocytes were elevated as early as 1 h, peaked at 6 h and remained high until 24 h (Fig. 1B) compared with controls. Intriguingly, western blotting analysis showed a significant increase in the levels of H3K181a from 3 to 12 h after UCB administration, with the largest increase occurring at 6 h, which correlated with changes in lactate levels in astrocytes (Fig. 1C). GlycoPER, which reflected glycolytic flux was further investigated to validate metabolic changes of UCB-treated primary astrocytes using a Seahorse XFe96. As shown in Fig. 1D-E, astrocytes exposed

to UCB for 6 h displayed higher levels of basic and compensatory glycolysis than the controls.

Compared with age-matched control rats, BE model rats showed higher lactate levels in hippocampus from post-modeling 1 to 7 days and reached their peak on day 5 (Fig. 1F). In line with the lactate levels, the relative expression of H3K181a was gradually increased in hippocampus regions of BE rats, and reached its greatest level on the 5th day after UCB injection (Fig. 1G). These findings are correlated with our previous reports that BE rats showed the most obvious pyroptosis on post-modeling day 7, which implies that H3K181a may regulate the expression of pyroptosis-associated proteins [15]. Considering the central role of hippocampus in learning and memory, subsequent experiments focused on this area. Based on these results, it can be concluded that lactate and H3K181a levels of astrocytes are increased in the context of BE.

Inhibition of H3K181a suppressed UCB-induced pyroptosis in primary cultured astrocytes, and hippocampus of BE rats

To evaluate whether H3K181a inhibition attenuated pyroptosis in astrocytes, a glycolysis inhibitor (OX) was adopted to reduce lactate production and H3K181a as previously reported [40]. In primary cultured astrocytes, the CCK8 assay was employed to assess the cell viability

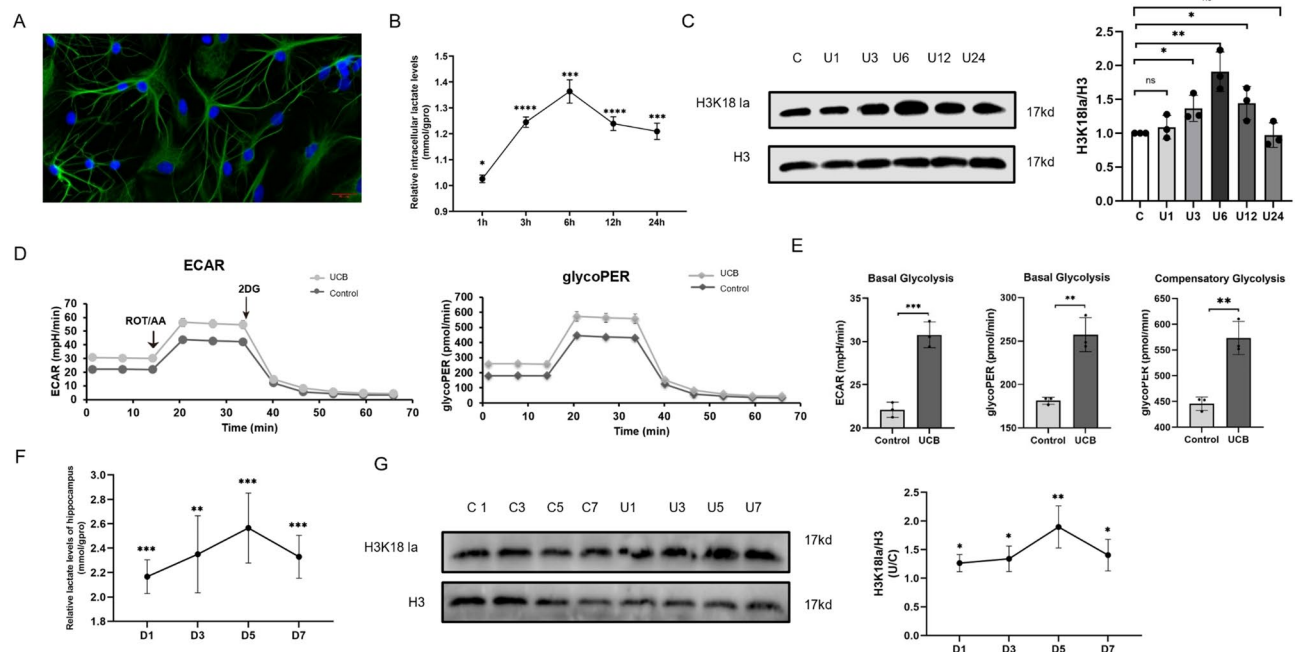


Fig. 1 H3K181a is elevated in UCB-exposed primary astrocytes and hippocampus tissues of BE rats. **(A)** Immunofluorescence staining image for GFAP (green). **(B)** The time-dependent changes of intracellular lactate levels in primary astrocytes at 0, 1, 3, 6, 12 and 24-h after UCB intervention. **(C)** Western blot analysis of H3K181a levels in primary astrocytes at 0, 1, 3, 6, 12 and 24-h after UCB stimulation. **(D-E)** ECAR and glycoPER of primary astrocytes with or without UCB challenge at 6 h followed by injections of Rot/AA (0.5 μ M), and 2-DG (50 mM). **(F)** The time-dependent changes of lactate levels in hippocampus tissues of BE rats at 1, 3, 5, and 7-day post-modeling. **(G)** Western blot analysis of H3K181a levels in hippocampus tissues of BE rats at 1, 3, 5, and 7-day post-modeling; C, Control group, U, UCB group. Data are presented as the mean \pm SD from three independent experiments. * $P < 0.05$, ** $P < 0.01$, *** $P < 0.001$ and **** $P < 0.0001$, ns, no significance

after pre-treatment with OX for 2 h, followed by co-cubation with UCB for 6 h. The results showed that 5 mM/L OX significantly reduced the cell survival rate in combination with UCB (Additional file 1: Fig. S1a), thus, lower doses were chosen in the following study. Notably, OX reduced intracellular lactate and H3K18la levels in primary cultured astrocytes in a dose-dependent manner (Additional file 1: Fig. S1b). Immunofluorescent staining further confirmed that 2.5 mM/L OX, acting as a lactate dehydrogenase inhibitor A (LDHA) inhibitor, reduced H3K18la in primary cultured astrocytes treated with UCB (Additional file 1: Fig. S1c). ELISA revealed that OX (2.5 mM/L) inhibited the UCB-induced expression of inflammatory factor IL-1 β (Additional file 1: Fig. S1d), and WB demonstrated the reduced pyroptosis-associated

proteins Caspase-1 p20, GSDMD-N and NLRP3 in primary cultured astrocytes (Additional file 1: Fig. S1e). Since OX may exert additional effects apart from inhibiting lactate production and lactylation, LDHA was further knocked down to inhibit H3K18la. After adding the si-LDHA and transfection reagent, RT-qPCR at 24 h and WB at 48 h confirmed that LDHA was successfully knocked down (Additional file 1: Fig. S1f-g). As expected, si-LDHA significantly impaired lactate production and histone lactylation (Fig. 2A, B, UCB + si-LDHA vs. UCB + NC, $P=0.0308$ for intracellular lactate; $P=0.0298$ for H3K18la), and triggered a significant inhibition of cellular pyroptosis (Fig. 2C, D, UCB + si-LDHA vs. UCB + NC, $P=0.0042$ for Caspase-1 p20; $P=0.0101$ for GSDMD-N; $P=0.0299$ for NLRP3). Next, sodium

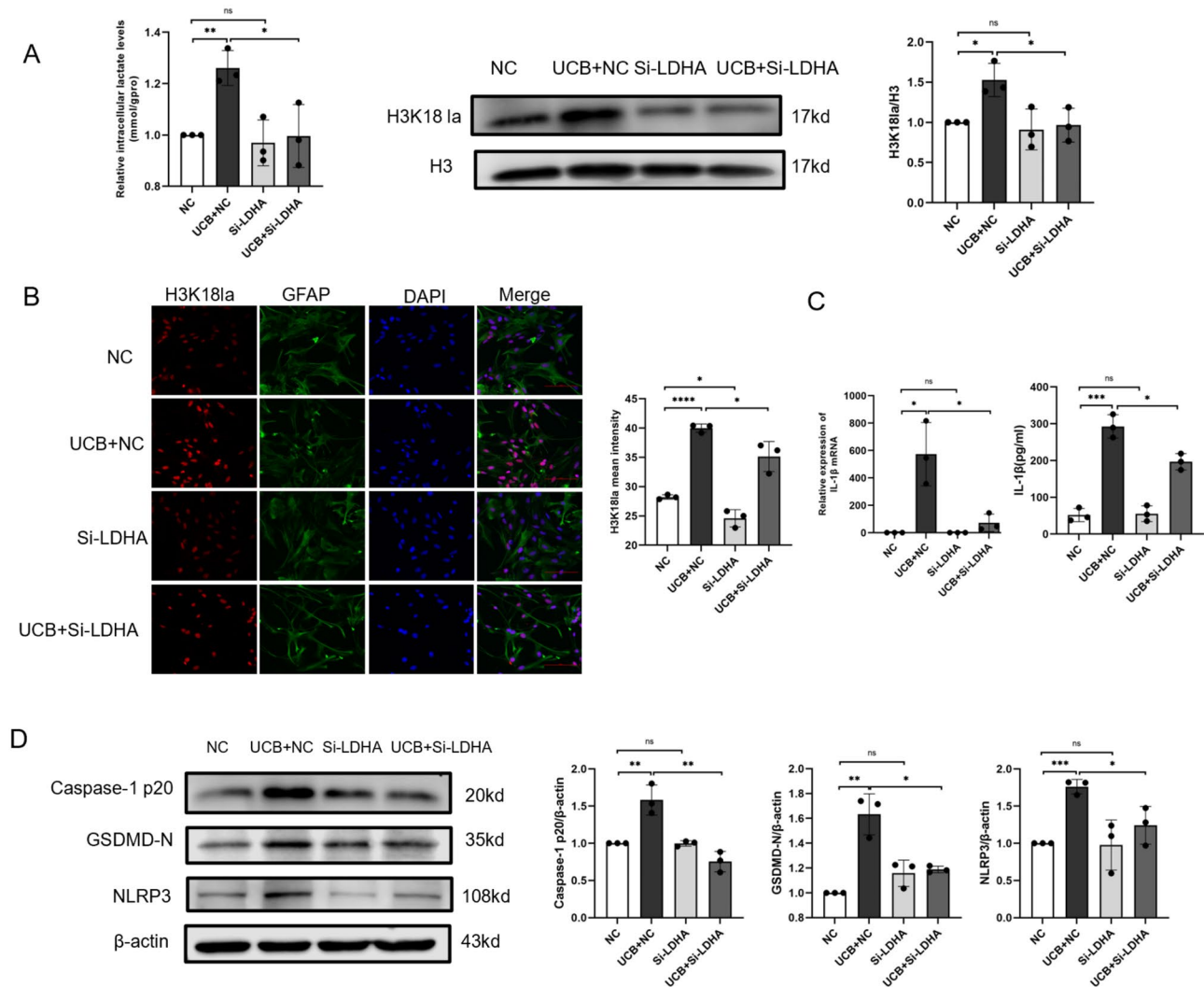


Fig. 2 Knock-down of LDHA reduces H3K18la levels and inhibits pyroptosis in primary astrocytes. **(A)** Intracellular lactate and H3K18la levels in UCB-induced astrocytes after transfection with si-NC or si-LDHA. **(B)** Immunofluorescence co-staining for H3K18la (red) and GFAP (green) in UCB-induced astrocytes after transfection with si-NC or si-LDHA. Scale bars: 100 μ m. **(C)** RT-qPCR and ELISA analysis of IL-1 β in UCB-exposed astrocytes after transfection with si-NC or si-LDHA. **(D)** Western blot analysis of Caspase-1 p20, GSDMD-N and NLRP3 levels in UCB-exposed astrocytes after transfection with si-NC or si-LDHA. Data are presented as the mean \pm SD from three independent experiments. * $P < 0.05$, ** $P < 0.01$, *** $P < 0.001$ and **** $P < 0.0001$, ns, no significance

lactate was applied to raise the level of histone lactylation in primary cultured astrocytes 1 h before UCB stimulation. It was found that 30 mM/L sodium lactate significantly reduced cell survival rate in UCB-exposed astrocytes (Additional file 1: Fig. S2a), thus, lower doses were utilized for the following study to increased intracellular lactate and H3K18la levels (Additional file 1: Fig. S2b). However, it was found that sodium lactate did not further enhance the levels of inflammatory factors and proteins related to pyroptosis (Additional file 1: Fig. S2c, d), suggesting that the increased pyroptosis induced by H3K18la may reach the maximum level.

As observed in in vitro experiments, OX significantly decreased the levels of lactate and H3K18la on the 5th day following UCB injection (Additional file 1: Fig. S3a, b), as well as the pyroptosis indicators on the 7th day in hippocampus tissues of BE rats (Additional file 1: Fig. S3c, d). Taken together, these findings indicate that inhibition of H3K18la alleviates UCB-induced pyroptosis in primary cultured astrocytes and hippocampus tissues of BE rats.

Identification of potential downstream targets of H3K18la

To investigate the potential regulatory role of H3K18la in gene expression, genome-wide CUT&Tag analysis in primary cultured astrocytes subjected to UCB was performed. The data revealed that H3K18la was enriched in promoter regions (Fig. 3A, Additional file 1: Fig. S4a). Kyoto Encyclopedia of Genes and Genomes (KEGG) analysis identified that genes' promoters bound by H3K18la were enriched in nervous system, immune system; infectious disease; and carbohydrate and glycan biosynthesis metabolism (Additional file 1: Fig. S4b), suggesting a regulatory effect of H3K18la in neuroinflammation. In addition, the top 20 KEGG pathways included mitogen-activated protein kinase (MAPK) and phosphatidylinositol 3-kinase/serine-threonine kinase (PI3K/AKT) signaling pathways that play critical roles in inflammation (Fig. 3B). Intriguingly, RNA sequencing (RNA-seq) data indicated that the top 20 KEGG analysis of upregulated genes in UCB-exposed primary astrocytes compared with controls was enriched in TNF signaling pathway, NF- κ B signaling pathway, IL-17 signaling pathway, NOD-like receptor signaling pathway, Toll-like receptor signaling pathway, JAK-STAT signaling pathway and C-type lectin receptor signaling pathway (Fig. 3C). Moreover, the top 20 KEGG analysis of downregulated genes in LDHA-deficient primary astrocytes under UCB intervention was enriched in infectious disease and pro-inflammatory immune signaling pathways, especially Toll-like receptor signaling pathway and NOD-like receptor signaling pathway (Fig. 3D). By comparing RNA-seq data described above, only Toll-like receptor signaling pathway and NOD-like receptor signaling

pathway levels were increased under UCB stimulation, and simultaneously decreased after LDHA knockdown in UCB-treated astrocytes, which suggests that H3K18la may regulate pyroptosis of astrocytes through these two signaling pathways. Since NOD-like receptor signaling pathway altered more significantly than Toll-like receptor signaling pathway, genes associated with this pathway were chosen as our focus. In addition, the gene expression of *Caspase-1 p20*, *GSDMD-N*, *NLRP3* and *IL-1 β* of NOD-like receptor signaling pathway in primary astrocytes exposed to UCB was reduced following LDHA knockdown, which was consistent with our preliminary findings mentioned above (Additional file 1: Table S4). Next, by combining CUT&Tag data with RNA-seq data of the transcriptome of UCB-exposed primary astrocytes undergoing LDA knockdown or not and the transcriptome of control and UCB-treated primary astrocytes, 16 H3K18la-binding genes with significantly reduced mRNA levels in UCB-exposed astrocytes experiencing LDHA interference and also highly expressed in UCB-subjected astrocytes were identified (Fig. 3E, Additional file 1: Table S5). All genes associated with the NOD-like receptor signaling pathway were obtained from the GeneCards database, and it was found that, among the 16 candidate genes, only *NOD2* is a member of NOD-like receptor signaling pathway; accordingly, we decided to focus on it.

A genomic snapshot revealed a significant enrichment of the H3K18la signal at the *NOD2* promoter (Fig. 3F). CUT&Tag qPCR also indicated that H3K18la enriched in *NOD2* promoter regions was increased in primary astrocytes treated with UCB compared with controls ($P=0.0048$), and by knocking down LDHA, this enrichment was reduced (Fig. 3G, $P=0.0395$). In line with expectations, mRNA (Fig. 3H) and protein (Fig. 3I, J) levels of *NOD2* were significantly increased in primary astrocytes after UCB intervention and decreased after transfection with si-LDHA. Collectively, these data suggest that the transcription of *NOD2* is positively regulated by H3K18la.

H3K18la promotes pyroptosis in primary cultured astrocytes exposed to UCB through NOD2/MAPK and NOD2/NF- κ B signaling pathways

To identify the effect of *NOD2* on UCB-induced pyroptosis, *NOD2* was knocked down in primary cultured astrocytes which was verified by RT-qPCR and WB (Additional file 1: Fig. S4c, d). It was observed that *NOD2* knockdown inhibited pyroptosis in primary astrocytes subjected to UCB (Fig. 4A, B, UCB + si-*NOD2* vs. UCB + NC, $P=0.0251$ for *Caspase-1 p20*; $P=0.0004$ for *GSDMD-N*; $P=0.0071$ for *NLRP3*), which indicates that *NOD2* plays a facilitating role in pyroptosis of UCB-exposed astrocytes. After overexpressing *NOD2*

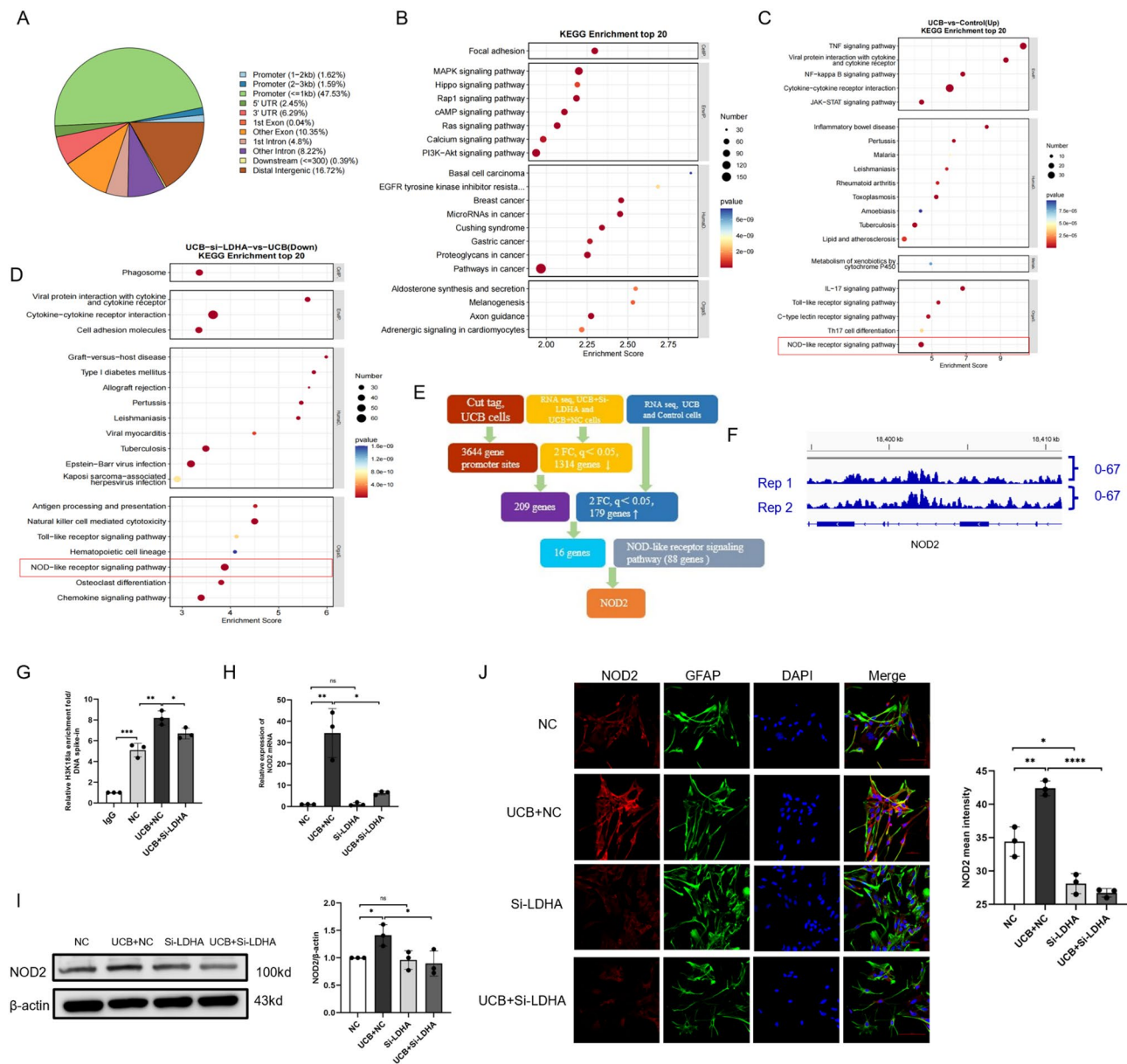


Fig. 3 H3K18la activates transcription of NOD2. **(A)** The genomic distribution of H3K18la sites. **(B)** KEGG analysis of H3K18la peaks. **(C)** KEGG analysis of upregulated genes in UCB-treated primary astrocytes compared with controls ($q < 0.05$, $FC > 1.5$). **(D)** KEGG analysis of downregulated genes after *LDHA* knockdown in UCB-treated primary astrocytes ($q < 0.05$, $FC > 2$). **(E)** Bioinformatics analysis filtered *NOD2* as a downstream target of H3K18la. **(F)** IGV tracks for *NOD2* from CUT& Tag analysis. **(G)** CUT&Tag-qPCR assay of H3K18la peaks bound to *NOD2*. **(H)** RT-qPCR analysis of *NOD2* in UCB-exposed astrocytes after being transfected with si-NC or si-LDHA. **(I–J)** Western blot analysis of *NOD2* and immunofluorescence co-staining for *NOD2* (red) and GFAP (green) in UCB-exposed astrocytes after transfection with si-NC or si-LDHA. Scale bars: 50–100 μm . Data are presented as the mean \pm SD from three independent experiments. * $P < 0.05$, ** $P < 0.01$, *** $P < 0.001$ and **** $P < 0.0001$, ns, no significance

in primary astrocytes (Additional file 1: Fig. S4e, f), the anti-pyoptosis effects of *LDHA* knockdown were partially compromised (Fig. 4C, D, $P = 0.0083$ for Caspase-1 p20; $P < 0.0001$ for GSDMD-N; $P = 0.0132$ for NLRP3). Altogether, these results suggest that H3K18la promotes pyroptosis partially through *NOD2* in UCB-exposed primary astrocytes.

NOD2 signals are transduced by activating the NF- κ B and the MAPK phosphorylation cascades through the

involvement of RIK2, which can ultimately increase pyroptotic proteins and chemokines expression (41, 42). Thus, *NOD2*/RIK2 axis, together with its well-established downstream pathways NF- κ B and MAPK, were identified as the signaling cascades to be investigated subsequently. WB showed that both si-LDHA and si-*NOD2* suppressed the increase of RIK2 and p-p65 expression induced by UCB in primary astrocytes, as well as the phosphorylation of JNK, ERK, and p-38 (Fig. 4E). Furthermore,

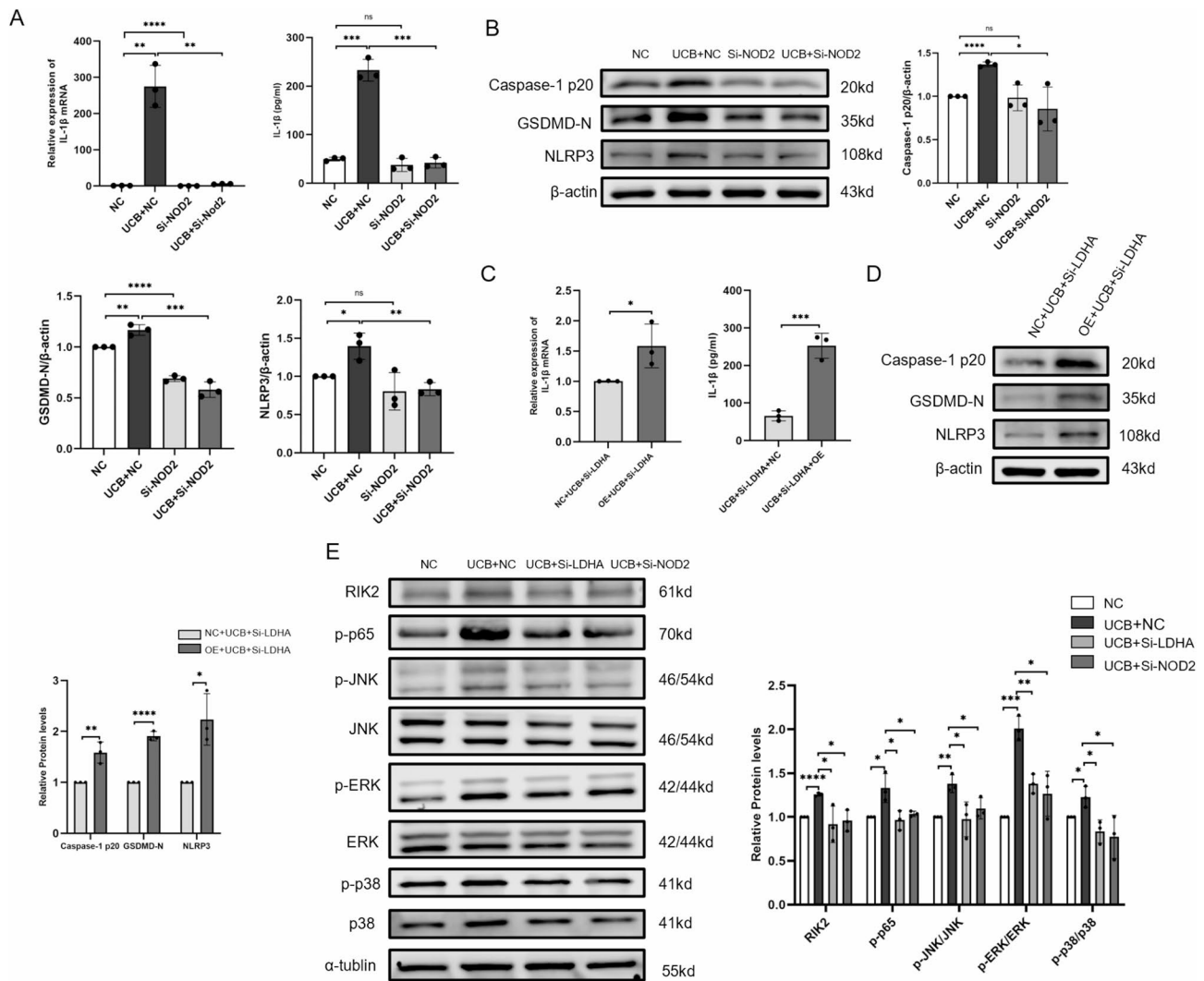


Fig. 4 H3K18la promotes pyroptosis in primary astrocytes through NOD2/MAPK and NOD2/NF- κ B signalling pathways. **(A)** RT-qPCR and ELISA analysis of IL-1 β in UCB-exposed astrocytes with or without *NOD2* knockdown. **(B)** Western blot analysis of Caspase-1 p20, GSDMD-N and NLRP3 levels in UCB-exposed astrocytes with or without *NOD2* knockdown. **(C)** RT-qPCR and ELISA analysis of IL-1 β in primary UCB-exposed astrocytes with or without *NOD2* overexpression after transfected with si-LDHA. **(D)** Western blot analysis of Caspase-1 p20, GSDMD-N and NLRP3 levels in primary UCB-exposed astrocytes with or without *NOD2* overexpression after LDHA knockdown. **(E)** Western blot analysis of RIK2, p-p65, p-JNK, JNK, p-ERK, ERK, p-p38 and p-38 levels in UCB-exposed astrocytes after LDHA or *NOD2* knockdown. Data are presented as the mean \pm SD from three independent experiments. * $P < 0.05$, ** $P < 0.01$, *** $P < 0.001$ and **** $P < 0.0001$, ns, no significance

LDHA knockdown-induced MAPK and NF- κ B pathways suppression could be rescued by gain of *NOD2* (Additional file 1: Fig. S4g). Altogether, these results imply that H3K18la/*NOD2*/MAPK and H3K18la/*NOD2*/NF- κ B axes contribute to UCB-induced pyroptosis in primary astrocytes.

H3K18la/*NOD2* signaling axis aggravates pyroptosis in hippocampus of BE rats by upregulating MAPK and NF- κ B signaling pathways

To further evaluate expression level of *NOD2* and the effects of H3K18la/*NOD2* axis as well as its downstream pathways on pyroptosis of hippocampus tissues, BE

model rats were established and hippocampus homogenates were extracted on the 7th day. WB and immunofluorescent staining showed an increased expression of *NOD2* after UCB injection (UCB vs. control, $P = 0.0009$ for immunofluorescent staining; $P = 0.0141$ for WB), whereas its expression was largely diminished by OX treatment simultaneously (Fig. 5A, B, UCB + OX vs. UCB, $P = 0.0012$ for immunofluorescent staining; $P = 0.0118$ for WB). Since the in vivo experiments in the first two parts of the results revealed that H3K18la level was elevated under UCB injection and OX treatment inhibited H3K18la level, it can be concluded that H3K18la plays a potential role in promoting *NOD2* expression in

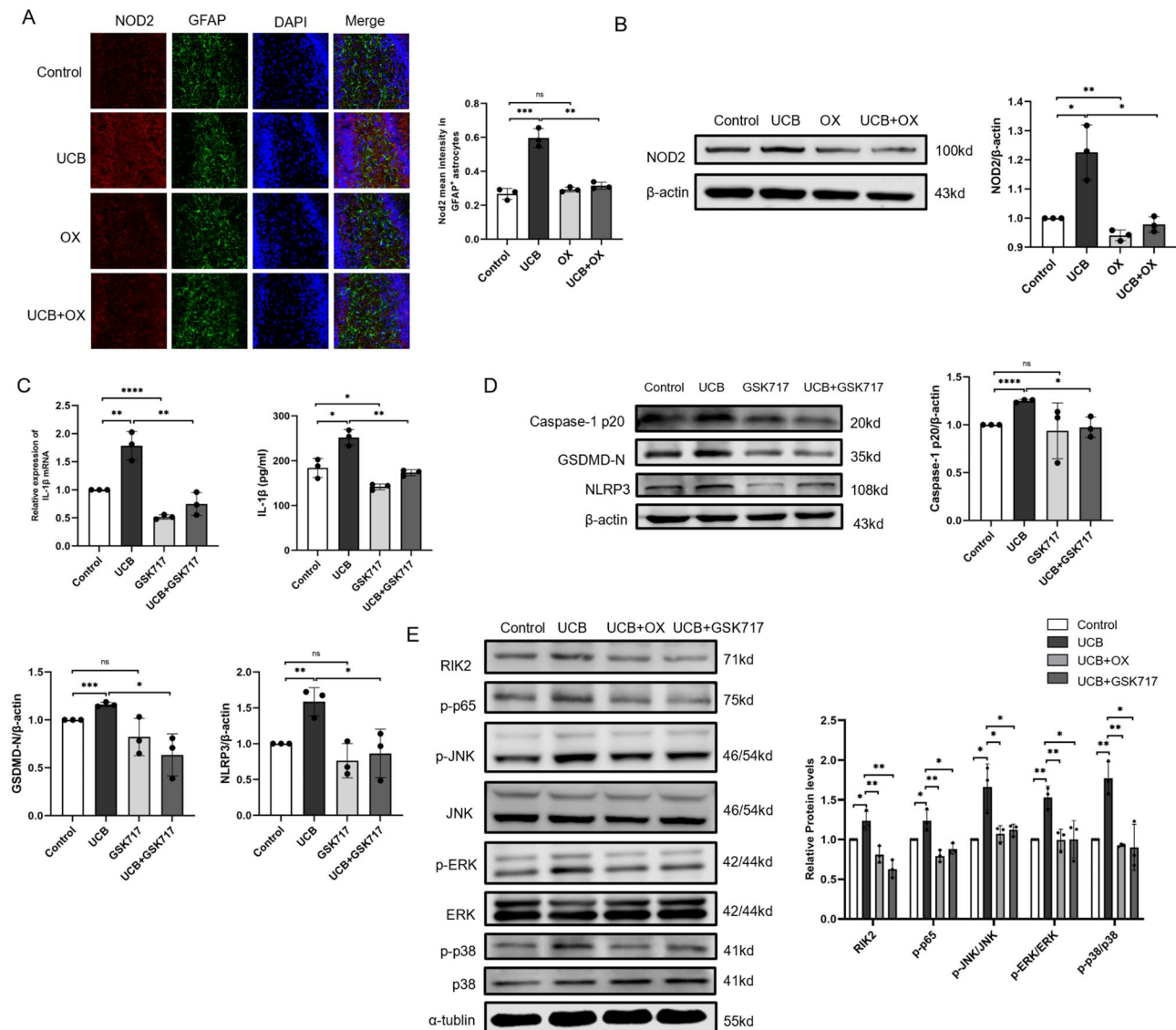


Fig. 5 H3K18la/NOD2 signaling axis aggravates pyroptosis in hippocampus of BE rats by upregulating MAPK and NF- κ B signaling pathways. **(A)** Immunofluorescence co-staining for NOD2 (red) and GFAP (green) in the hippocampal DG region of BE rats after OX intervention. Scale bars: 100 μ m. **(B)** Western blot analysis of NOD2 in the hippocampus of BE rats after OX intervention. **(C)** RT-qPCR and ELISA analysis of IL-1 β in hippocampus tissues of BE rats after GSK717 treatment. **(D)** Western blot analysis of Caspase-1 p20, GSDMD-N and NLRP3 levels in hippocampus tissues of BE rats after GSK717 treatment. **(E)** Western blot analysis of RIK2, p-p65, p-JNK, JNK, p-ERK, ERK, p-p38 and p-38 levels in hippocampus tissues of BE rats after OX or GSK717 administration. Data are presented as the mean \pm SD from three independent experiments. * P < 0.05, ** P < 0.01, *** P < 0.001 and **** P < 0.0001, ns, no significance

hippocampus tissues of BE rats. Next, GSK717, a selective NOD2 inhibitor, was employed to probe into the potential role of NOD2 in pyroptosis of hippocampus tissues of BE rats. RT-qPCR, ELISA and WB results showed that the expression of pyroptosis-related components (IL-1 β , GSDMD-N, Caspase-1 p20 and NLRP3) induced by UCB exposure were partially reduced by GSK717 administration (Fig. 5C, D). Furthermore, protein levels of MAPK and NF- κ B pathways were downregulated by LDHA inhibitor (OX) as well as NOD2 inhibitor (GSK717) (Fig. 5E). In summary, these findings support that H3K18la/NOD2/MAPK and H3K18la/NOD2/

NF- κ B axes are involved in pyroptosis of hippocampus in BE rats.

Inhibition of H3K18la alleviates neuronal injury and improves long-term neurological functions of BE rats

To assess the neuroprotective effects of inhibiting H3K18la on UCB-induced neuronal damage, H&E staining was performed on brain sections of BE rats 7 days after modeling. In the control group, the DG region of the hippocampus and cortex showed intact neurons, with lightly stained cytoplasm and large vesicular nuclei. In contrast, the UCB group displayed a marked increase in

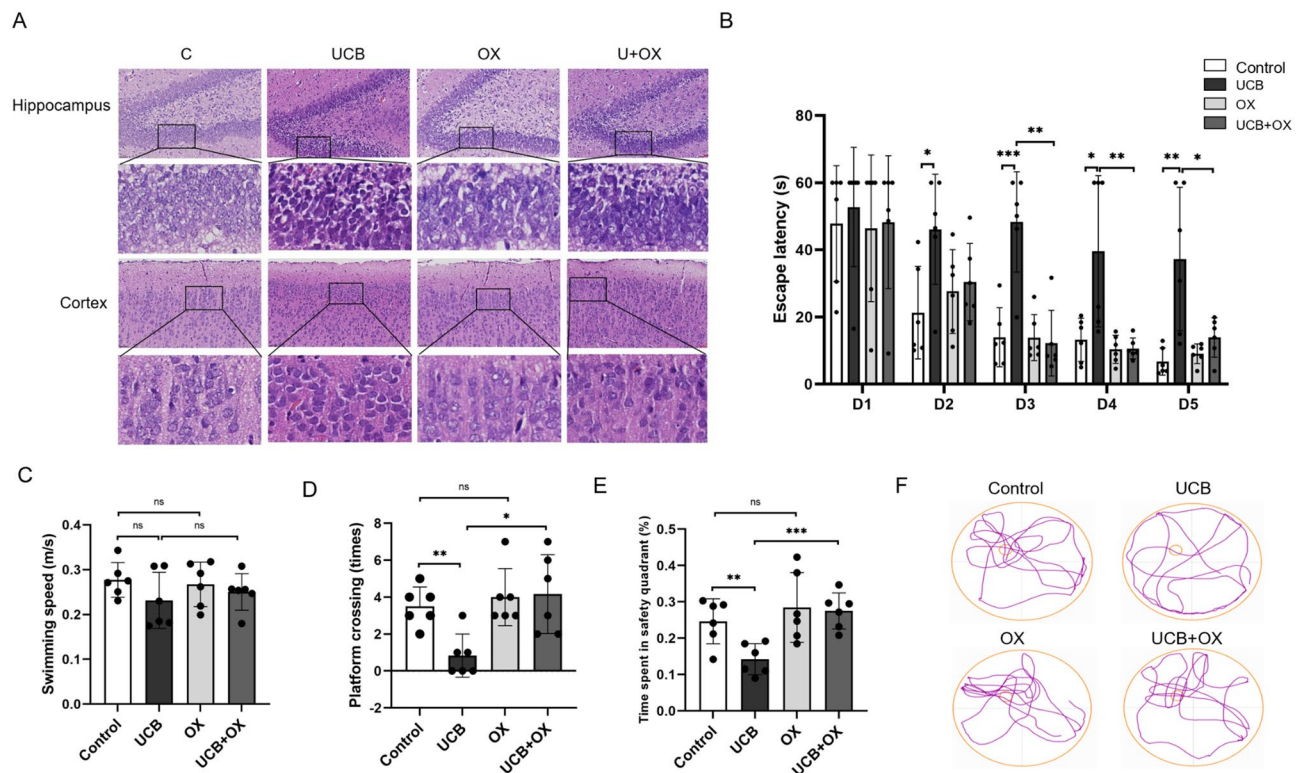


Fig. 6 Inhibition of H3K18la by OX alleviates neuronal injury and improves spatial learning and memory in BE rats. **(A)** H&E staining showing morphologic alteration of neurons in the brain cortex and hippocampal DG region on post-modeling day 7. Scale bars: 25 μ m. **(B)** Latency to find the platform during the training days of the MWM test. **(C)** Swimming speed among all groups during the probe testing of the MWM test on day 6. **(D)** The crossing times during the probe trial of the MWM test on day 6. **(E)** Time spent in the target quadrant during the probe trial of the MWM test on day 6. **(F)** Representative swimming paths of model rats during the probe trial in the MWM test. Data are presented as the mean \pm SD from six independent experiments. * $P < 0.05$, ** $P < 0.01$, and *** $P < 0.001$, ns, no significance

necrotic neurons characterized by nuclear pyknosis and shrunken neuronal bodies. Importantly, treatment with OX rescued neuronal damage of the hippocampus and cortex induced by UCB (Fig. 6A).

In order to demonstrate whether OX administration alleviated the spatial learning and memory performance of BE rats, the Morris water maze test (MWM) was conducted on 28-day-old model rats. In the training trials, the UCB group had significantly longer escape latency on days 2–5 compared with the control group, while OX treatment attenuated this cognitive impairment, as evidenced by shorter escape latency on day 3 to day 5 of MWM training (Fig. 6B). In the probe trial, all the rats showed similar swim distance and swim speed in the test (Fig. 6C). The UCB group exhibited decreased frequency of platform crossings ($P = 0.0087$) and proportions of time spent in the safety quadrant ($P = 0.0068$) compared to the control group, while BE rats treated with OX showed a significant increase in both indices compared to the UCB group (Fig. 6D, E, $P = 0.0130$ for platform crossings; $P = 0.0006$ for time spent in the safety quadrant). These findings indicate that inhibition of H3K18la

can be understood as a potential strategy for improving neurological function in BE.

Discussion

As the most abundant and diverse types of glial cells, astrocytes are essential for developing neuronal networks, maintaining homeostasis and modulating the immune responses of the central nervous system (CNS) [43, 44]. An increasing number of studies have shown that astrocytes possess distinct histone modifications that underlie their acquisition of identity and plasticity, contributing to development of neurological disorders [45–47]; for example, a newly discovered memory astrocyte subset controlled by histone acetylation promotes CNS pathology [46]. Recently, a new type of histone modification, called histone lactylation, was identified [31], but its role in astrocytes has not been thoroughly studied. Since astrocytes show a high preference for lactate-directed glycolysis which is similar to the metabolic process in proliferating cancer cells [48], this research explored the underlying role of histone lactylation in astrocytic immune response. The present study identified that astrocytes under UCB stimulation presented

with elevated levels of lactate and H3K18la, and inhibition of histone lactylation efficiently attenuated UCB-induced pyroptosis *in vivo* and *in vitro*. In the epigenetic mechanism, elevated H3K18la promoted the expression of NOD2 and its downstream pathways of MAPK and NF- κ B, thereby aggravating neuroinflammation, neuronal injury and neurological function impairment of BE rats.

The innate immune response serves as the body's first line of defense against endogenous stress and pathogens, and this rapid and non-specific response depends upon recognition by pathogen recognition receptors (PRRs) [49]. As a family of intracellular PRRs, NLRs are divided into four subfamilies: NLRA, NLRB, NLRC and NLRP. NOD1 and NOD2 receptors, which are both NLRC proteins, were the first identified NLRs and were initially found to recognize specific structures within bacterial peptidoglycan [50, 51]. However, increasing evidence suggests that NOD1 and NOD2, besides the recognition of pathogen-associated molecular patterns (PAMPs), can also participate in recognition of damage-associated molecular patterns (DAMPs) including environmental signals and endogenous byproducts of cellular damage, resulting in subsequent activation of NF- κ B and MAPK phosphorylation cascades [42]. For instance, a recent study showed that Decabromodiphenyl ethane (DBDPE), a widespread pollutant in the environment, activated the NLRP3 inflammasome in human aortic endothelial cells by upregulating the NOD2/RIK2/NF- κ B signaling pathway [52]. Keestra-Gounder et al. [53] discovered that endoplasmic reticulum (ER) stress inducers triggered production of the pro-inflammatory cytokine IL-6 in a NOD1/2-dependent fashion, which implies that NOD1 and NOD2 signaling pathways link ER stress with inflammation. Furthermore, *in vivo* and *in vitro* observations indicate that the known inflammatory signaling pathways of NF- κ B and MAPK activation are critical common events among detrimental responses of astrocytes [44], and were proved to be activated by UCB [37, 54–55]. Consistent with the findings mentioned above, this study demonstrated that UCB as a sterile inflammatory stimulus activated the expression of NOD2 in a peptidoglycan-independent way, and upregulated inflammatory responses of astrocytes via both NF- κ B and MAPK pathways.

In the present, there is still controversy over whether lactylation plays a pro-inflammatory or anti-inflammatory role in immune cells. Since Zhao et al. [31] discovered that elevated lysine lactylation (Kla) is related to transition of macrophage from inflammatory (M1) to reparatory state (M2), which is characterized by high levels of arginase1 (Arg1), subsequent studies have also reached similar conclusions in dextran sulfate sodium (DSS)-induced colitis, sepsis, myocardial infarction

and various tumors [32, 56]. However, Dichtl et al. [57] questioned the association of increased lactylation with anti-inflammatory genes expression in macrophage as described by Zhang and others. According to them, LPS-induced Arg1 was reliant on interleukin 6 (IL-6) signal transduction without K_{la} involved, while lactylation was positively correlated with different modes of macrophages death in PANoptosis. In addition, some other research indicated that lactate-derived lactylation plays a pro-inflammatory role in sepsis, lung fibrosis and sepsis-associated lung injury etc [32, 58]. As shown above, the role of lactylation in inflammatory response of macrophages remains inconclusive, and further studies are required. As for neuropsychiatric disorders, a majority of evidence identified that increased lactylation drives pro-inflammatory cell activation and neuroinflammation including AD [34, 59], Schizophrenia [60] and Parkinson's disease [61]. In agreement with the previous findings regarding the nervous system, the current work observed that enhanced H3K18la level caused by lactate accumulation in UCB-exposed astrocytes triggered amplified inflammatory signaling cascades which resulted in pyroptosis, thereby contributing to the development of BE. In contrast, a recently reported study found that decreased H4K8la level exacerbated astrocyte reactivity after subarachnoid hemorrhage in mice, suggesting an inhibitory effect of lactylation on astrocyte inflammatory responses [62]. Differences in lysine lactylation sites and disease models may explain the different findings between this study and ours. Moreover, this study used only male mice and did not investigate the specific mechanism by which lactylation modulates astrocyte polarization; so the findings in this study need to be further validated.

Lactate derived from astrocytic glycolysis has a double-edged effect on the regulation of nervous system function, which may be due to the activation of different signaling pathways, different intervention durations and dose-related effects of lactate. According to the known astrocyte–neuron lactate shuttle (ANLS) model and subsequent relevant studies, it is believed that lactate is transferred from astrocytes to neurons to fulfill the neuronal energetic needs, as well as provide signals that modulate neuronal functions including plasticity, excitability and memory consolidation [63]. However, there is also a large body of research reporting that lactate is detrimental for CNS disorders including ischemia, traumatic brain injury, psychiatric disorders and neurodegenerative diseases [63–66]. In addition, a recent meta-analysis from 281 human datasets revealed that gene expression alterations associated with decreased pH are over-represented in 11 brain diseases, and astrocytes express the most acidity-related genes in type-specific analyses [67]. Consistent with the findings mentioned above, this present study found that enhanced lactate level caused by

UCB-exposed primary astrocytes exacerbated neuroinflammation through epigenetic mechanism. According to clinical observations, bilirubin neurotoxicity can be exacerbated by comorbidities with acidosis in neonates [68]. Current hypotheses for this clinical phenomenon include that acidosis increases blood-brain barrier permeability and elevates the susceptibility to bilirubin-induced toxicity in neurons [69], but whether lactylation derived from lactate in astrocytes is also part of the underlying mechanism remains to be further investigated. Taken together, it is reasonable to speculate that the elevated lactate and histone lactylation caused by glycolysis of UCB-exposed astrocytes play a detrimental role in the context of BE.

The study, however, has some limitations that cannot be ignored. Firstly, previous studies have reported that NOD2 can be regulated by DNA methylation and histone acetylation [70, 71], while the interaction or competition between the 2 epigenetic modifications and histone lactylation was not explored in the current study and requires further investigation. Secondly, communication with CNS-resident and CNS-recruited cells is critical to the modulation of astrocytic homeostatic functions and disease-associated responses, which were not investigated in the present research. Thus, it would be intriguing to examine how enhanced lactate and histone lactylation levels in astrocytes impact surrounding cells, especially microglia and neurons, and whether this lactate-dependent histone modification contributes to the synergistic cytotoxicity to neurons in neonates experiencing hyperbilirubinemia concurrent with acidosis.

Conclusions

In summary, the current study demonstrates a novel molecular mechanism in which H3K18la/NOD2 axis modulates UCB-induced neuroinflammation. Findings in this study will provide an important complement to metabolic-epigenetic understandings in astrocytes. Therefore, inhibition of glycolysis in astrocytes may be a potential therapeutic strategy for the treatment of neuroinflammation-related diseases.

Supplementary Information

The online version contains supplementary material available at <https://doi.org/10.1186/s12974-025-03399-2>.

Supplementary Material 1

Supplementary Material 2

Author contributions

ZYH, JL, and SYL conceived the study and designed the experiments. JL, SYL, QS, and YZ performed the experiments. ZYH and JL analyzed the data and drafted the manuscript. All authors reviewed and approved the final manuscript.

Funding

This research was supported by the National Natural Science Foundation of China (Grant No. 81971426) and the Postgraduate Research Innovation Project of Chongqing (Grant No. CYB23209 and CYB22213), the Key Project for Technological Innovation and Application Development of Chongqing (Grant No. CSTB2022TIAD-KPX0147) and the Science and Technology Research Program of Chongqing Municipal Education Commission (Grant No. KJZD-M202300403).

Data availability

All data needed to evaluate the conclusions in the paper are present in the paper or the Supplementary Materials. CUT&Tag (PRJNA1159477) and RNA-seq data (PRJNA1141236 and PRJNA1155856) are available through the National Center for Biotechnology Information Gene Expression Omnibus.

Declarations

Ethics approval and consent to participate

All animal experiments were approved by the Animal Care Professional Committee of Chongqing Medical University (permit number: SYXK2022-0016). No human studies are involved in this study.

Competing interests

The authors declare no competing interests.

Author details

¹Department of Neonatology, Children's Hospital of Chongqing Medical University, National Clinical Research Center for Child Health and Disorders, Ministry of Education Key Laboratory of Child Development and Disorders, Chongqing, China

²Chongqing Key Laboratory of Child Rare Diseases in Infection and Immunity, Chongqing, China

Received: 14 August 2024 / Accepted: 24 February 2025

Published online: 12 March 2025

References

1. Chu L, Xue X, Qiao J. Efficacy of intermittent phototherapy versus continuous phototherapy for treatment of neonatal hyperbilirubinaemia: A systematic review and Meta-analysis. *J Adv Nurs*. 2021;77:12–22.
2. Olusanya BO, Kaplan M, Hansen T. Neonatal hyperbilirubinaemia: a global perspective. *Lancet Child Adolesc*. 2018;2:610–20.
3. Mitra S, Rennie J. Neonatal jaundice: aetiology, diagnosis and treatment. *Brit J Hosp Med*. 2017;78:699–704.
4. Bhutani VK, Stark AR, Lazzaroni LC, et al. Predischarge screening for severe neonatal hyperbilirubinemia identifies infants who need phototherapy. *J Pediatr -Us*. 2013;162:477–82.
5. Bhutani VK, Wong R. Bilirubin-induced neurologic dysfunction (BIND). *Semin Fetal Neonat M*. 2015;20:1.
6. Olusanya BO, Ogunlesi TA, Slusher TM. Why is Kernicterus still a major cause of death and disability in low-income and middle-income countries? *Arch Dis Child*. 2014;99:1117–21.
7. Greco C, Arnolda G, Boo NY, et al. Neonatal jaundice in Low- and Middle-Income countries: lessons and future directions from the 2015 don Ostrow Trieste yellow retreat. *Neonatology*. 2016;110:172–80.
8. Deliktas M, Ergin H, Demiray A, et al. Caffeine prevents bilirubin-induced cytotoxicity in cultured newborn rat astrocytes. *J Matern-Fetal Neo M*. 2019;32:1813–9.
9. Vodret S, Bortolussi G, Iaconcig A, et al. Attenuation of neuro-inflammation improves survival and neurodegeneration in a mouse model of severe neonatal hyperbilirubinemia. *Brain Behav Immun*. 2018;70:166–78.
10. Vodret S, Bortolussi G, Jasprova J, et al. Inflammatory signature of cerebellar neurodegeneration during neonatal hyperbilirubinemia in Ugt1 (-/-) mouse model. *J Neuroinflamm*. 2017;14:64.
11. Fernandes A, Silva RF, Falcao AS, et al. Cytokine production, glutamate release and cell death in rat cultured astrocytes treated with unconjugated bilirubin and LPS. *J Neuroimmunol*. 2004;153:64–75.
12. Vaz AR, Falcao AS, Scarpa E, et al. Microglia susceptibility to free bilirubin is Age-Dependent. *Front Pharmacol*. 2020;11:1012.

13. Liu X, Zhang Z, Ruan J, et al. Inflammasome-activated gasdermin D causes pyroptosis by forming membrane pores. *Nature*. 2016;535:153–8.
14. Feng J, Li M, Wei Q, et al. Unconjugated bilirubin induces pyroptosis in cultured rat cortical astrocytes. *J Neuroinflamm*. 2018;15:23.
15. Li S, Huang H, Wei Q, et al. Depression of pyroptosis by inhibiting Caspase-1 activation improves neurological outcomes of Kernicterus model rats. *Acs Chem Neurosci*. 2021;12:2929–39.
16. Verkhratsky A, Nedergaard M. Physiology of astroglia. *Physiol Rev*. 2018;98:239–389.
17. Linnerbauer M, Wheeler MA, Quintana FJ. Astrocyte crosstalk in CNS inflammation. *Neuron*. 2020;108:608–22.
18. Patani R, Hardingham GE, Liddelow SA. Functional roles of reactive astrocytes in neuroinflammation and neurodegeneration. *Nat Rev Neurol*. 2023;19:395–409.
19. Robb JL, Hammad NA, Weightman PP, et al. The metabolic response to inflammation in astrocytes is regulated by nuclear factor-kappa B signaling. *Glia*. 2020;68:2246–63.
20. Pamies D, Sartori C, Schwart D, et al. *Int J Mol Sci* 2021; 22.
21. Vizueté A, Froes F, Seady M, et al. Early effects of LPS-induced neuroinflammation on the rat hippocampal glycolytic pathway. *J Neuroinflamm*. 2022;19:255.
22. Borbor M, Yin D, Brockmeier U, et al. Neurotoxicity of ischemic astrocytes involves STAT3-mediated metabolic switching and depends on glycogen usage. *Glia*. 2023;71:1553–69.
23. Das NS, Sousa JC, Magalhaes R, et al. Astrocytes undergo metabolic reprogramming in the multiple sclerosis animal model. *Cells-Basel* 2023; 12.
24. Andersson AK, Ronnback L, Hansson E. Lactate induces tumour necrosis factor-alpha, interleukin-6 and interleukin-1beta release in microglial- and astroglial-enriched primary cultures. *J Neurochem*. 2005;93:1327–33.
25. Hu W, Cheng X, Ye X, et al. Ex vivo (1)H nuclear magnetic resonance spectroscopy reveals systematic alterations in cerebral metabolites as the key pathogenetic mechanism of bilirubin encephalopathy. *Mol Brain*. 2014;7:87.
26. Supplie LM, Duking T, Campbell G, et al. Respiration-Deficient astrocytes survive as glycolytic cells in vivo. *J Neurosci*. 2017;37:4231–42.
27. Dienel GA, Cruz NF. Aerobic Glycolysis during brain activation: adrenergic regulation and -influence of norepinephrine on astrocytic metabolism. *J Neurochem*. 2016;138:14–52.
28. Goyal MS, Hawrylycz M, Miller JA, et al. Aerobic Glycolysis in the human brain is associated with development and neonatal gene expression. *Cell Metab*. 2014;19:49–57.
29. Flavahan WA, Gaskell E, Bernstein BE. Epigenetic plasticity and the hallmarks of cancer. *Science* 2017; 357.
30. Sabari BR, Zhang D, Allis CD, et al. Metabolic regulation of gene expression through histone acylations. *Nat Rev Mol Cell Bio*. 2017;18:90–101.
31. Zhang D, Tang Z, Huang H, et al. Metabolic regulation of gene expression by histone lactylation. *Nature*. 2019;574:575–80.
32. Liu X, Zhang Y, Li W, et al. Lactylation, an emerging hallmark of metabolic reprogramming: current progress and open challenges. *Front Cell Dev Biol*. 2022;10:972020.
33. Chu X, Di C, Chang P, et al. Lactylated histone H3K18 as a potential biomarker for the diagnosis and predicting the severity of septic shock. *Front Immunol*. 2021;12:786666.
34. Wei L, Yang X, Wang J, et al. H3K18 lactylation of senescent microglia potentiates brain aging and Alzheimer's disease through the NFKappaB signaling pathway. *J Neuroinflamm*. 2023;20:208.
35. Yao X, Li C. Lactate dehydrogenase A mediated histone lactylation induced the pyroptosis through targeting HMGb1. *Metab Brain Dis*. 2023;38:1543–53.
36. Li S, Huang H, Zhang Y, et al. Bilirubin induces A1-Like reactivity of astrocyte. *Neurochem Res*. 2023;48:804–15.
37. Fernandes A, Falcao AS, Silva RF, et al. Inflammatory signalling pathways involved in astroglial activation by unconjugated bilirubin. *J Neurochem*. 2006;96:1667–79.
38. Falcao AS, Fernandes A, Brito MA, et al. Bilirubin-induced immunostimulant effects and toxicity vary with neural cell type and maturation state. *Acta Neuropathol*. 2006;112:95–105.
39. Song S, Hu Y, Gu X, et al. A novel newborn rat Kernicterus model created by injecting a bilirubin solution into the cisterna magna. *PLoS ONE*. 2014;9:e96171.
40. Yu J, Chai P, Xie M, et al. Histone lactylation drives oncogenesis by facilitating m(6)A reader protein YTHDF2 expression in ocular melanoma. *Genome Biol*. 2021;22:85.
41. Griffin ME, Espinosa J, Becker JL, et al. Enterococcus peptidoglycan remodeling promotes checkpoint inhibitor cancer immunotherapy. *Science*. 2021;373:1040–6.
42. Trindade BC, Chen GY. NOD1 and NOD2 in inflammatory and infectious diseases. *Immunol Rev*. 2020;297:139–61.
43. Han RT, Kim RD, Molofsky AV, et al. Astrocyte-immune cell interactions in physiology and pathology. *Immunity*. 2021;54:211–24.
44. Colombo E, Farina C, Astrocytes. Key regulators of neuroinflammation. *Trends Immunol*. 2016;37:608–20.
45. Pavlou M, Grandbarbe L, Buckley NJ, et al. Transcriptional and epigenetic mechanisms underlying astrocyte identity. *Prog Neurobiol*. 2019;174:36–52.
46. Lee HG, Rone JM, Li Z, et al. Disease-associated astrocyte epigenetic memory promotes CNS pathology. *Nature*. 2024;627:865–72.
47. Sardar D, Cheng YT, Woo J, et al. Induction of astrocytic Slc22a3 regulates sensory processing through histone serotonylation. *Science*. 2023;380:eade0027.
48. Vaupel P, Multhoff G. Revisiting the Warburg effect: historical dogma versus current Understanding. *J Physiol -London*. 2021;599:1745–57.
49. Kawai T, Akira S. The roles of TLRs, RLRs and NLRs in pathogen recognition. *Int Immunol*. 2009;21:317–37.
50. Inohara N, Ogura Y, Chen FF, et al. Human Nod1 confers responsiveness to bacterial lipopolysaccharides. *J Biol Chem*. 2001;276:2551–4.
51. Ogura Y, Inohara N, Benito A, et al. Nod2, a Nod1/Apa-1 family member that is restricted to monocytes and activates NF-kappaB. *J Biol Chem*. 2001;276:4812–8.
52. Jing L, Zheng D, Sun X, et al. DBDPE upregulates NOD-like receptor signaling to induce NLRP3 inflammasome-mediated HAECs pyroptosis. *Environ Pollut*. 2023;318:120882.
53. Keestra-Gounder AM, Byndloss MX, Seyffert N, et al. NOD1 and NOD2 signalling links ER stress with inflammation. *Nature*. 2016;532:394–7.
54. Li M, Song S, Li S, et al. The Blockade of NF-kappaB activation by a specific inhibitory peptide has a strong neuroprotective role in a Sprague-Dawley rat Kernicterus model. *J Biol Chem*. 2015;290:30042–52.
55. Fernandes A, Brites D. Contribution of inflammatory processes to nerve cell toxicity by bilirubin and efficacy of potential therapeutic agents. *Curr Pharm Des*. 2009;15:2915–26.
56. Zhu W, Guo S, Sun J, et al. Lactate and lactylation in cardiovascular diseases: current progress and future perspectives. *Metabolism*. 2024;158:155957.
57. Dichtl S, Lindenthal L, Zeitler L, et al. Lactate and IL6 define separable paths of inflammatory metabolic adaptation. *Sci Adv*. 2021;7.
58. Shu M, Lu D, Zhu Z, et al. Insight into the roles of lactylation in macrophages: functions and clinical implications. *Clin Sci (Lond)*. 2025; 139(2).
59. Pan RY, He L, Zhang J, et al. Positive feedback regulation of microglial glucose metabolism by histone H4 lysine 12 lactylation in Alzheimer's disease. *Cell Metab*. 2022;34:634–48.
60. Xie J, Hong S, Zhang X, et al. Inhibition of Glycolysis prevents behavioural changes in mice with MK801-induced SCZ model by alleviating lactate accumulation and lactylation. *Brain Res*. 2023;1812:148409.
61. Qin Q, Wang D, Qu Y, et al. Enhanced glycolysis-derived lactate promotes microglial activation in Parkinson's disease via histone lactylation. 2023. <https://www.researchsquare.com/article/rs-3249462/v1>
62. Zhang F, Zhou J, Lu P, et al. Lactylation of histone by BRD4 regulates astrocyte polarization after experimental subarachnoid hemorrhage. *J Neuroinflamm*. 2024;21:186.
63. Magistretti PJ, Allaman I. Lactate in the brain: from metabolic end-product to signalling molecule. *Nat Rev Neurosci*. 2018;19:235–49.
64. Mason S. Lactate shuttles in Neuroenergetics-Homeostasis, allostasis and beyond. *Front Neurosci-Switz*. 2017;11:43.
65. Cauli B, Dusart I, Li D. Lactate as a determinant of neuronal excitability, neuroenergetics and beyond. *Neurobiol Dis*. 2023;184:106207.
66. Nohesara S, Abdolmaleky HM, Thiagalangam S. Potential for new therapeutic approaches by targeting lactate and pH mediated epigenetic dysregulation in major mental diseases. *Biomedicines*. 2024;12.
67. Hagihara H, Murano T, Miyakawa T. The gene expression patterns as surrogate indices of pH in the brain. *Front Psychiatry*. 2023;14:1151480.
68. Alexandra BM, Silva RF, Brites D. Bilirubin toxicity to human erythrocytes: a review. *Clin Chim Acta*. 2006;374:46–56.
69. Lai K, Song XL, Shi HS, et al. Bilirubin enhances the activity of ASIC channels to exacerbate neurotoxicity in neonatal hyperbilirubinemia in mice. *Sci Transl Med*. 2020;12:eaax1337.
70. Leung CH, Lam W, Ma DL, et al. Butyrate mediates nucleotide-binding and oligomerisation domain (NOD) 2-dependent mucosal immune responses against peptidoglycan. *Eur J Immunol*. 2009;39:3529–37.

71. Feerick CL, McKernan DP. DNA methyltransferase inhibitors increase NOD-like receptor activity and expression in a monocytic cell line. *Immunopharm Immunot.* 2022;44:99–109.

Publisher's note

Springer Nature remains neutral with regard to jurisdictional claims in published maps and institutional affiliations.